Effect of implanted metal impurities on superconducting tungsten films

B. A. Young[a)]
Department of Physics, Santa Clara University, Santa Clara, California 95053

T. Saab, B. Cabrera, A. J. Miller, P. L. Brink and J. P. Castle
Department of Physics, Stanford University, Stanford, California 94305

(Received 10 December 2001; accepted for publication 24 February 2002)

The superconducting transition temperature of more than 30 thin-film tungsten samples was measured using a dilution refrigerator. The samples were fabricated using a 99.999% pure tungsten target and a dc magnetron sputtering system. Individual films were then doped with metal impurity ions using an accurate ion implantation technique. The effect of the metal–ion doping on the superconducting transition temperature was measured for samples with superconducting transitions in the range of 40–150 mK. Magnetic dopant species including Ni, Co, and Fe resulted in suppressed values of the tungsten T_c. The suppression was linear with increasing dopant concentration, for concentrations up to tens of ppm. For higher concentrations of magnetic atoms, the data are consistent with the Abrikosov–Gor'kov theory [Soviet Physics JETP **12**, 1243 (1961)] modified by antiferromagnetic impurity–impurity interactions. By contrast, tungsten films implanted with Mg or Cr showed little change in T_c after doping. In this article, we present data from cryogenic experiments on these films. We also present x-ray diffraction (XRD) spectra for a subset of the films. Our XRD data confirm that the observed suppression in T_c for the magnetically doped samples is not due to any structural changes (e.g., lattice distortion or damage) induced by the implantation process. [DOI: 10.1063/1.1469690]

INTRODUCTION

Our initial interest in adding magnetic impurity atoms to high-purity superconducting tungsten films was motivated by a need for thin-film phonon sensors with adjustable superconducting transition temperature T_c. The phonon sensors are used for experiments in particle astrophysics.[1] The performance of these sensors depends critically on the T_c of the superconducting W film, and also on the width of the superconducting transition.[2] We succeeded in developing T_c-tunable tungsten sensors for our applications, and the results of that work have been published.[3] At the time that work was done, we were unaware that other groups had previously published magnetic-impurity data for nontungsten superconducting systems.[4] In this article, we extend our earlier results with implanted iron to include two other magnetic dopant species: cobalt and nickel. We also report on results obtained with nonmagnetic ''control'' species: magnesium and chromium.

The tungsten films used in the studies described below were deposited using a Balzers 450 dc magnetron sputtering system. The as-deposited tungsten films from this system tend to be predominantly polycrystalline, bcc tungsten; this morphology for tungsten is often referred to as its low T_c phase, or alpha phase. Our films also contain a small amount of the metastable, high T_c phase, or beta phase, of tungsten; this is an A15 structure that tends to form when oxygen is present during the deposition.[5] Our as-deposited films have superconducting transition temperatures of the desired order of magnitude for our work (we aim for $T_c \approx 65$ mK). However, the films often have T_c values closer to 150 mK, which is too high for our present applications. We attribute the observed variability in T_c from one batch of films to the next to differing stress characteristics in the deposited films and/or to minute quantities of various residual impurities present in our vacuum chamber during deposition, and/or to other process parameters not yet identified. Fortunately, although the exact cause of the T_c variability has proven difficult to identify and completely remove, the T_c variability itself is easily corrected for in postprocessing, by magnetically doping our otherwise fully fabricated devices. Moreover, our robust technique for adjusting the sharp T_c of our films using ion implantation of magnetic ions does not broaden the superconducting transition nor degrade device performance.

SAMPLES

The samples used in this work were taken from a 350-Å-thick tungsten film deposited on a 210-Å-thick layer of amorphous silicon, on top of a polished, 76-mm-diam, (100) silicon wafer. The presence of the amorphous silicon layer was not important from the standpoint of these studies; it was included for reasons related to the operation of our actual full-scale devices in applications experiments. The amorphous silicon layer and the tungsten film were deposited sequentially without breaking vacuum in the sputtering chamber. The sputtering target used to deposit all of our tungsten films was purchased from Johnson Matthey. It is a 99.999% pure, vacuum-pressed, tungsten target that contains residual impurity concentrations of 0.07 ppm Mg, 0.3 ppm Cr, 0.9 ppm Fe, 0.0019 ppm Co, and 0.10 ppm Ni.

a)Author to whom correspondence should be addressed; electronic mail: byoung@scuacc.scu.edu

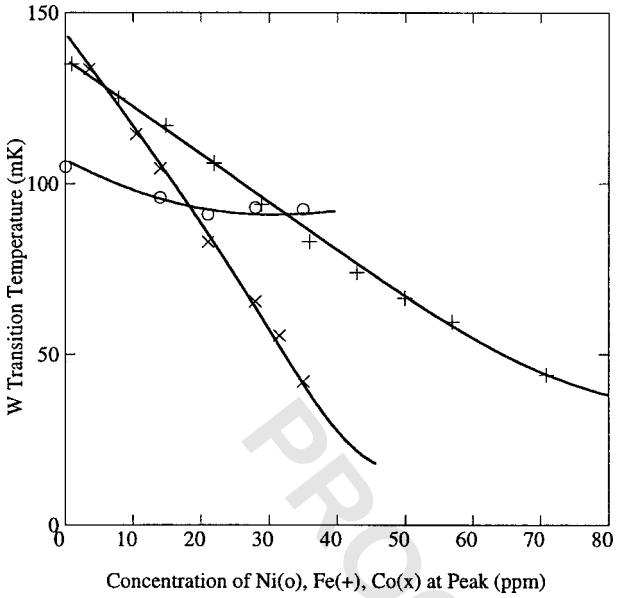

FIG. 1. Measured superconducting transition temperature of 350-Å-thick tungsten films doped with either $^{56}Fe^{+}(+)$, $^{59}Co^{+}(\times)$, or $^{58}Ni^{+}(\bigcirc)$. The curves correspond to the Abrikosov–Gor'kov model modified with antiferromagnetic ordering between dopant atoms. The parameters of the separate fits are given in Table I.

For each set of experiments described below, at least eight neighboring pieced taken from the central region of a single metallized ''test'' wafer were used; this allowed us to have one ''control'' sample from the wafer and seven or more ''test'' samples. The uniformity of T_c across the metallized wafer was good; ± 4 mK across the 7.6-mm-diam wafer. Each sample was ≈ 0.25 cm^2 in area. The test samples were separately implanted with the ions of choice, using a Varian ion implanter which has been modified to accommodate nontraditional ion sources. The ion beam energies used were 25 and 47 keV for $^{24}Mg^{+}$ and $^{52}Cr^{+}$, respectively, and 50 keV for $^{56}Fe^{+}$, $^{59}Co^{+}$, and $^{58}Ni^{+}$. Doses ranging from 1.00×10^{12} to 5.00×10^{13} ions/cm^2 ($\pm 0.01\%$) were used in the studies presented here. All implants were performed with a 7° wafer tilt with respect to the incoming beam. The beam energies were chosen so that the peak of the implanted ion distribution would appear approximately 40% of the way into the 350-Å-thick tungsten film. For reference, the superconducting coherence length in our tungsten films is $\xi_0 \approx 0.3$ μm, which is much greater than the film thickness ≈ 350 Å.

TABLE I. Values of the magnetic coupling parameter α, the critical concentration x_c and the superconducting transition temperature corresponding to zero impurity atoms of a specific impurity species T_{c0}. The values given correspond to three thin-film systems studied: iron-doped tungsten, cobalt-doped tungsten, and nickel-doped tungsten.

	Fe–W	Co–W	Ni–W
α	−0.060	−0.020	−1.0
x_c (ppm)	69	38	72
T_{c0} (mK)	136	144	107

TABLE II. Calculated values of the Abrikosov–Gor'kov and Ruderman–Kittel–Kasuya–Yosida spin-flip relaxation parameters τ_{AG} and τ_{RKKY} for our ion-doped samples of thin-film tungsten.

	Fe–W (K^{-1})	Co–W (K^{-1})	Ni–W (K^{-1})
$\tau_{AG}(x_c)$	7.6	6.5	12
$\tau_{RKKY}(x_c, T_{c0})$	−130	−325	−12

T_c RESULTS AND ANALYSIS—Fe, Ni, AND Co

In Fig. 1, we plot the measured T_c of our 350-Å-thick tungsten films versus dopant concentration for three different magnetic ion species: $^{56}Fe^{+}$, $^{59}Co^{+}$, and $^{58}Ni^{+}$. Three differ-

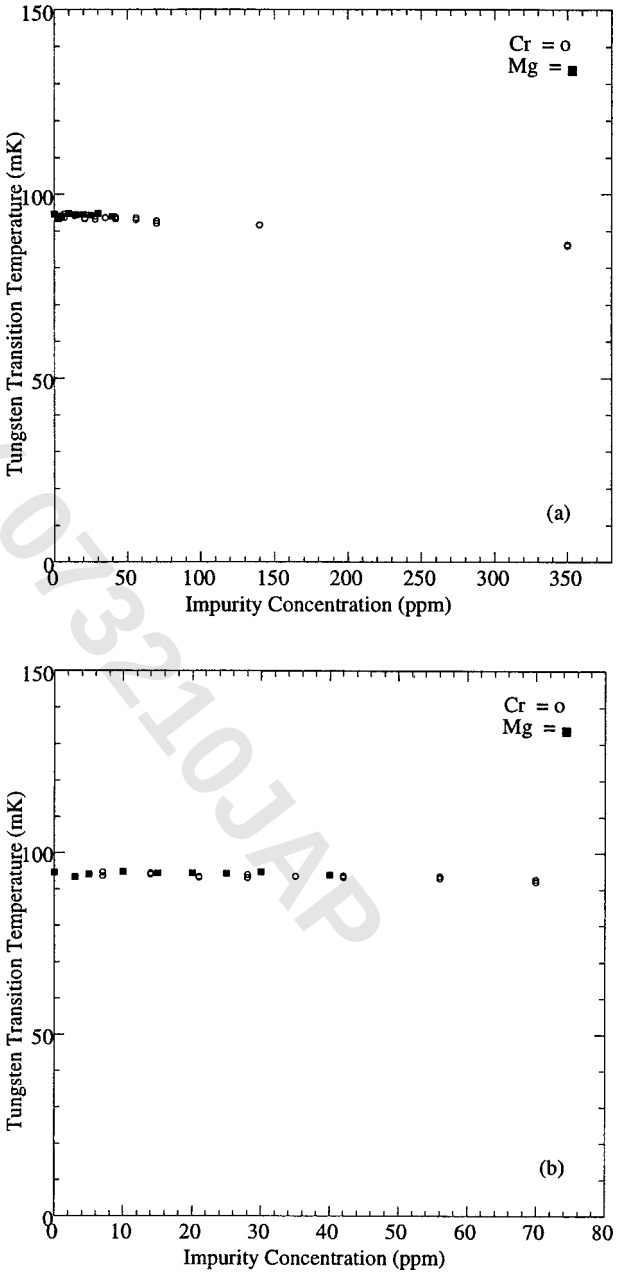

FIG. 2. Measured superconducting transition temperature as a function of dopant concentration for nonparamagnetic dopant atoms Mg (●) and Cr (○) in 350-Å-thick tungsten films. (a) Full range of dopant concentration studied. (b) Expanded view of low concentration region shown in (a).

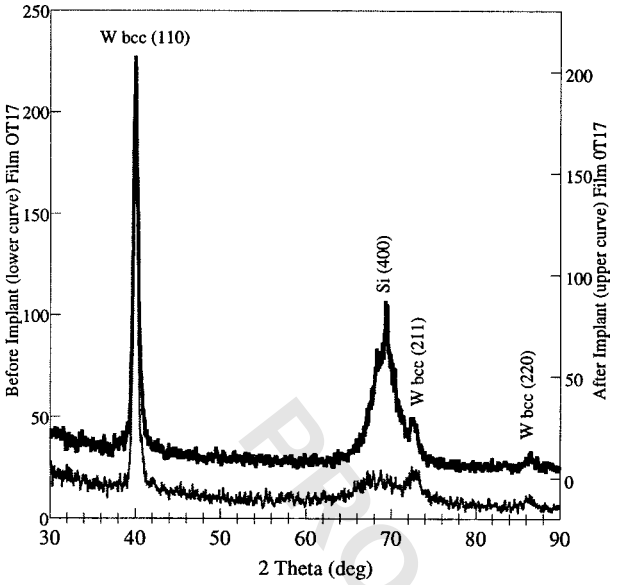

FIG. 3. XRD spectrum for a 350 Å tungsten film (sample OT17) before (lower curve) and after (upper curve) implantation with $3.6\times10^{12}/\text{cm}^2$ $^{56}\text{Fe}^+$ at 50 keV. The unimplanted sample (lower curve) had a superconducting T_c of 135 mK. The implanted sample (upper curve) had a superconducting T_c of 95 mK. We identify three tungsten peaks corresponding to (110), (211), and (220) planes of bcc tungsten. The broad structure near 69° is attributed to substrate events.

ent wafers were used for this study, one for each implanted ion species. Thus, the three different unimplanted ''control'' samples (one from each wafer) had different values of T_c.

The curves shown in Fig. 1 correspond to a fit based on the theoretical prediction of Abrikosov and Gor'kov (AG)

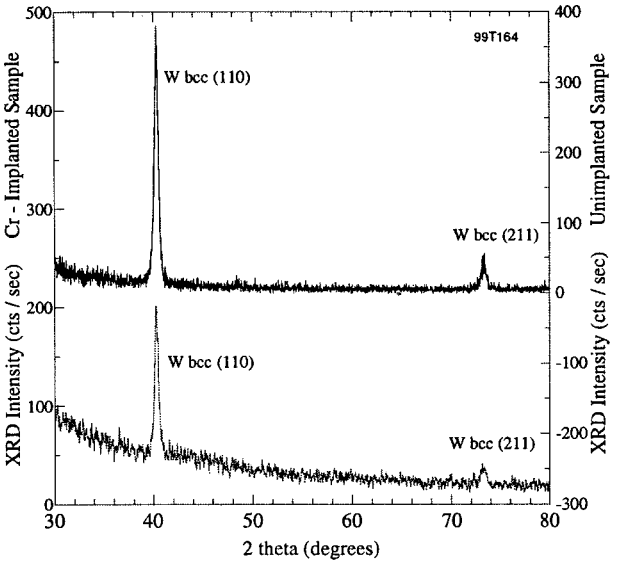

FIG. 4. XRD spectra obtained with a 350-Å-thick tungsten film (sample 99T164) both before (upper curve) and after (lower curve) implantation with a high dose of $5.0\times10^{13}/\text{cm}^2$ $^{52}\text{Cr}^+$ at 47 keV. This film had an undoped superconducting T_c of 95 mK. The peaks present in the spectra correspond to (110) and (211) bcc tungsten. The broad background distribution on the lower curve is due to x rays scattered off of a glass mounting slide used in the XRD measurement of the Cr-implanted sample. Compared to our results with dopants Co and Fe, little reduction in T_c was observed for tungsten films doped with the nonparamagnetic species Mg and Cr.

TABLE III. Values of the lattice parameter a for four films measured using XRD. All tungsten thin films used in this study had an as-deposited bcc structure. The films retained the bcc structure after ion doping.

	OT17 undoped W	OT17 doped W	99T164 undoped W	99T164 doped W
Measured T_c	135 mK	95 mK	95 mK	86 mK
Implant species	none	25 ppm Fe	none	350 ppm Cr
Lattice parameter a	3.18 Å	3.18 Å	3.16 Å	3.16 Å

for the general dependence of T_c on magnetic-impurity concentration.[6] In our analysis, the AG model is modified at high dopant concentrations by the inclusion of a term corresponding to antiferromagnetic ordering between nearest-neighbor magnetic impurities introduced by implantation. The ''high dopant-concentration limit corresponds to $T_c \ll T_{c0}$, where T_{c0} is the superconducting film T_c corresponding to 0 ppm of a specific impurity. Including these effects, the theoretical prediction of the behavior of T_c with magnetic ion doping concentration x is given by[3,7]

$$\ln(T_c/T_{c0}) = \Psi\{1/2\} - \Psi\{(1/2) + (1/4)(e^{-\gamma})(x/x_c) \times (T_{c0}/T_c)[1+\alpha(x/x_c)(T_{c0}/T_c)]\},$$

where Ψ is the digamma function and γ is the Euler–Mascheroni constant. In this equation, α is a magnetic coupling parameter which is defined in terms of the Abrikosov–Gor'kov and Ruderman–Kittel–Kasuya–Yosida (RKKY) spin-flip relaxation parameters τ_{AG} and τ_{RKKY}:

$$\alpha = \tau_{\text{AG}}(x_c)/\tau_{\text{RKKY}}(x_c, T_{c0}).$$

The relaxation parameters give the relative strengths of the impurity atom–host atom (e.g., Co–W) and the impurity atom–impurity atom (e.g., Co–Co) interactions, respectively.[7] Values of $\alpha>0$ correspond to ferromagnetic ordering (parallel spins) in a film; values of $\alpha<0$ correspond to antiferromagnetic ordering (antiparallel spins). Magnetic ordering in superconductors is discussed in depth in Refs. 6–10.

The critical concentration x_c is evaluated from the slope of the T_c versus x curve in the low concentration limit

$$\left.\frac{dT_c}{dx}\right|_{x=0} \cong \frac{-\pi^2}{8e^{\gamma}}\frac{T_{c0}}{x_c}.$$

In Table I we present values of α, x_c, and T_{c0} determined from our data for each of the three systems studied in this work:

Using the data summarized in Fig. 1 and Table I, we can readily calculate τ_{AG} and τ_{RKKY} for the Fe–W, Co–W, and Ni–W systems studied. In the dilute dopant limit

$$\left.\frac{dT_c}{dx}\right|_{x=0} = \frac{\pi}{4\tau_{\text{AG}}x}.$$

Thus, the results of Table II are obtained.

T_c RESULTS AND ANALYSIS—Mg AND Cr

In a followup series of experiments, we fabricated and tested tungsten samples implanted with nonmagnetic ions of

Mg and Cr. These samples were used to confirm that the T_c suppression effect evident in Fig. 1 was not simply a result of lattice damage induced by the ion implantation process itself. For these studied, 25 keV $^{24}Mg^+$ ions or 47 keV $^{52}Cr^+$ ions were implanted into high-purity 350-Å-thick tungsten films. The beam kinetic energies and ion doses were chosen so that the resulting implanted impurity distributions would be quantitatively similar to the distributions used in the magnetic ion experiments. For the Mg work, the impurity concentration at the peak of each implanted ion distribution was in the range of 3–40 ppm. For each Cr-implanted sample, the peak impurity concentration had a value between 7 and 350 ppm. The measured T_c values of the Mg–W and Cr–W samples are presented as a function of dopant concentration in Fig. 2.

FILM STRUCTURE MEASUREMENTS

X-ray diffraction (XRD) analysis was performed for several of our tungsten thin-film samples. In Fig. 3, we show the XRD results for a 350-Å-thick tungsten film both before (lower curve) and after (lower curve) implantation with $^{56}Fe^+$ at 50 keV. The measured T_c values of these samples were 135 mK (before implantation) and 95 mK (after implantation).

In Fig. 4, we show an XRD spectrum of an ''as-deposited,'' unimplanted tungsten film with $T_c=95$ mK (upper curve), and an XRD spectrum obtained using an immediately adjacent sample from the same metallized wafer after the sample was implanted with the nonparamagnetic dopant $^{52}Cr^+$ (lower curve). The data shown in this figure were filtered using a Stineman smoothing function before plotting. The Cr implantation was performed at 47 keV, with a dose of 5×10^{13} ions/cm^2. The poorer signal-to-noise ratio obtained with the Cr-implanted sample was a result of that sample's smaller size, which was comparable to the collimated x-ray beam profile ($\approx$2.5 mm$\times$1 mm) used for the XRD measurements. The continuous background that rises toward small scattering angles in the spectra of Fig. 4 originates from x rays scattering off an amorphous (glass) backing plate used to mount the small samples in the diffractometer.

The XRD data can be used to calculate the lattice spacing of our tungsten films before and after implantation. Our measurements were made using a Philips MRD diffractometer in the parallel-beam configuration. Assuming an incident x-ray source wavelength $\lambda=1.5418$ Å, corresponding to a weighted average of the K_α lines of Cu, and identifying the crystallographic peaks as shown in Figs. 3 and 4, we get for the lattice parameter of our thin-film samples the values shown in Table III. Our results are in good agreement with the reported value of 3.165 Å for bulk α-phase tungsten.[11]

ACKNOWLEDGMENTS

B.Y. thanks The Research Corporation and The Clare Boothe Luce Foundation for their support of this work from its beginning. Additional funding was provided by the Department of Energy under Grant No. DE-FG03-90ER40569. The tungsten films were sputterred at the Stanford Nanofabrication Facility; a National Science Foundation Technology Center housed in the Center for Integrated Systems at Stanford University. R. Atkins participated in some of the XRD measurements. T.S. acknowledges additional support from FCAR of Quebec, Canada.

[1] R. A. Abusaidi *et al.*, Phys. Rev. Lett. **84**, 5695 (2000); D. Abrams *et al.* Phys. Rev. D. (submitted).
[2] K. D. Irwin *et al.*, Appl. Phys. Lett. **66**, 1998 (1995); B. Cabrera, Nucl. Instrum. Methods Phys. Res. A **444**, 304 (2000); K. D. Irwin *et al.*, Rev. Sci. Instrum. **66**, 5322 (1995).
[3] B. A. Young, T. Saab, B. Cabrera, J. J. Cross, R. M. Clarke, and R. A. Abusaidi, J. Appl. Phys. **86**, 6975 (1999); B. A. Young, T. Saab, B. Cabrera, J. J. Cross, and R. A. Abusaidi, Nucl. Instrum. Methods Phys. Res. A **444**, 296 (2000).
[4] T. Habisreuther, W. Miehle, A. Plewnia, and P. Ziemann, Phys. Rev. B **46**, 14566 (1992-II); R. Schleif, M. Hitzfeld, P. Ziemann, W. Buckel, in *LT-17*, edited by U. Eckern, A. Schmid, W. Weber, and H. Wuhl (Elsevier Science, B. V., New York, 1984), p. 1269; A. Hofmann, W. Bauriedl, and P. Ziemann, Z. Phys. B: Condens. Matter **46**, 117 (1982); J. E. Smith, Jr. and D. M. Ginsberg, Phys. Rev. **167**, 345 (1968).
[5] Y. G. Shen, Y. M. Mai, Q. C. Zhang, D. R. McKenzie, W. D. McFall, and W. E. McBride, J. Appl. Phys. **87**, 177 (2000); Y. G. Shen, Y. W. Mai, W. E. McBride, D. R. McKenzie, and Q. C. Zhang, Appl. Phys. Lett. **75**, 2211 (1999); I. A. Weerasekera, S. I. Shah, D. V. Baxter, and K. M. Unruh, *ibid.* **64**, 3231 (1994); S. Basavaiah and S. R. Pollack, *ibid.* **12**, 259 (1968).
[6] A. A. Abrikosov and L. P. Gor'kov, Sov. Phys. JETP **12**, 1243 (1961).
[7] W. A. Roshen and J. Ruvalds, Phys. Rev. B **31**, 2929 (1985).
[8] M. B. Maple, in *Superconductivity in d- and f- Band Metals*, AIP Conference Proceedings, edited by D. H. Douglass (American Institute of Physics, NY, 1972), p. 175; M. B. Maple, Appl. Phys. **9**, 179 (1976).
[9] P. Fulde and J. Keller, in *Superconductivity in Ternary Compounds II*, edited by M. B. Maple and O. Fischer (Springer, New York, 1982), p. 249.
[10] W. Dupont, E. Ziemniak, and K. D. Usadel, J. Low Temp. Phys. **52**, 41 (1983).
[11] *ASM Metals Reference Book*, edited by M. Bauccio (American Society for Metals, Metals Park, OH, 1994).